Automated Optimization of Variable Back-Pressure of Scroll Compressors Across the Entire Operation Envelope

Christian BUSCH[1*], Markus ÖTTL[1]

[1] OBRIST Engineering GmbH,
Lustenau, Austria
+43(0)557762370, c.busch@obrist.at

* Corresponding Author

ABSTRACT

In the course of the electrification of vehicle drives, the requirements for thermal management systems are currently being redefined completely. This has a significant impact on the operating envelope of the compressor as the most important component in them. In addition to standard A/C operation, large cooling capacities and mass flows at high evaporation temperatures are needed for fast charging, while heat pump mode is characterized by low suction pressures and high pressure ratios. These new tasks significantly increase the required stable pressure and speed ranges of scroll compressors, which are de facto standard in most electrified mobile applications. A particularly complex engineering task and potentially major time bottleneck is tuning a variable back-pressure system, which most modern scroll compressors rely on for axial compliance between fixed and orbiting scroll. Natural refrigerants, especially the transcritical use of R744, for example, require an even more precise back-pressure tuning than usual. The work at hand will show how ultra-fast exact analytical geometry calculations and 1D thermodynamic flow simulations are combined in a fully automated optimization process to solve the task of ensuring proper back-pressure over the entire operating envelope of a scroll compressor. To have such an efficient and lean simulation toolchain is the key to being able to react in an environment of ever-changing boundary conditions and allows rapid development and investigation of new machine concepts and variants.

1. INTRODUCTION

Since its beginnings, the development of scroll compressors has made continuous progress thanks to innovative approaches of the engineers and scientists involved. After Creux (1905) introduced the concept of the scroll compressor, it took until the mid-1970s for the topic to be taken up again, but then with astonishing speed of development. Solutions for difficult problems were developed, highlighting self-adjusting mechanisms for radial and axial compensation, the latter introducing back-pressure systems. An optimized back-pressure significantly improves the overall performance of the scroll compressor by ensuring sufficient axial sealing with minimal friction. Early computational models to simulate the back-pressure behavior were shown by Tojo *et al.* (1986), Nieter *et al.* (1992), and Ooi *et al.* (1996). Particularly, in the present case of a transcritical R744 compressor, the interaction of various design aspects must be correctly coordinated. High pressure differences and resulting loads do not allow for a deviation from the optimum design. For example, having an axial compliance mechanism, it is crucial to find a back-pressure setting that works across the entire working envelope early in the design phase of the machine. This study is intended to show how the path from the definition of the geometry to the calculation of the required back-pressure force could look in detail. All calculations are integrated in a software tool using Matlab and the 1D flow simulation software GT-Suite.

2. GEOMETRY

The mathematical definition of the spiral geometry is the cornerstone for all further steps in the derivation and calculation of the geometric variables of the scroll compressor.

2.1 Parameterization Function of Planar Curves

Since the contribution of Gravesen and Henriksen (2001) to the theory of the geometry of scroll compressors, it has been shown that it is one the most flexible and versatile methods. Their introduction of a novel reference frame together with the concept of parameterizing the local curvature radius by a function of the tangent angle was an outstanding

simplification of a more general approach to define the spiral wrap geometry. It uses an intrinsic function which links arc length s and the tangential direction φ by a differential equation: $\frac{\mathrm{d}s}{\mathrm{d}\varphi} = \rho(\varphi)$ where ρ is the radius of curvature. Full advantage can be taken of this definition if ρ is a polynomial or piecewise polynomial function of φ as proposed first by Gravesen and subsequently used by many other authors, *e. g.* Bell *et al.* (2010). The main advantage is that almost all of the subsequent variables can be derived in closed analytical form, which leads to an immense acceleration of the calculation speed.

2.2 Scroll Wrap Definition

In this work, second order polynomials have been chosen to represent the scroll geometry curves. Compared to linear functions, which would reproduce ordinary circle involutes, the additional flexibility can be used to derive variable wall-thickness wrap designs, which are of great importance, especially for mobile applications. Third order representations are shown by Shaffer *et al.* (2012) for example. This, however, would significantly complicate the closed-form expressions without significantly increasing design flexibility. The proposed method uses two curves on the orbiting scroll which are defined independently of each other with a unique parameter set:

$$\mathbf{X} \rightarrow \ \rho(\varphi) = a\varphi^2 + b\varphi + c \qquad\qquad \mathbf{Y} \rightarrow \ \rho(\varphi) = d\varphi^2 + e\varphi + f \tag{1}$$

using the six parameters $a \ldots f$ for the two curves **X** and **Y** which together define the wall on the orbiting scroll. In the case a and d are equal to zero, once again circle involutes are obtained. The equations for the representation in Cartesian coordinates are calculated by integrating the above functions as shown by Gravesen and canceling out any constants, so, *e. g.* the **X** curve's coordinates can be written as the result of the matrix dot product:

$$\mathbf{X} = \begin{pmatrix} \cos(\varphi) & \sin(\varphi) \\ \sin(\varphi) & -\cos(\varphi) \end{pmatrix} \cdot \begin{pmatrix} 2a\varphi + b \\ a(\varphi^2 - 2) + b\varphi + c \end{pmatrix} = \begin{pmatrix} (2a\varphi + b)\cos\varphi + (a(\varphi^2 - 2) + b\varphi + c)\sin\varphi \\ (2a\varphi + b)\sin\varphi - (a(\varphi^2 - 2) + b\varphi + c)\cos\varphi \end{pmatrix} \tag{2}$$

2.3 Mating Curves

The equations for the corresponding mating curves on the fixed scroll are derived using Gravesen's method of adding a circular orbit offset. This offset is equal to the value of the scroll compressor's eccentricity r and can be positive or negative, depending on which direction is selected. By definition, a negative offset is applied on curve **X** which creates the curve **XN** on the fixed scroll, and a positive offset is applied on curve **Y** which leads to the curve **YP**, respectively. Hence, for example the coordinates of the curve **XN** are:

$$\mathbf{XN} = \begin{pmatrix} (2a\varphi + b)\cos\varphi + (a(\varphi^2 - 2) + b\varphi + c - r)\sin\varphi \\ (2a\varphi + b)\sin\varphi - (a(\varphi^2 - 2) + b\varphi + c - r)\cos\varphi \end{pmatrix} \tag{3}$$

To form the working chambers, the two orbiting curves are translated into a circular orbit relative to the fixed scroll curves by adding a vector $\vec{r} = r\,(\cos(-\alpha), \sin(-\alpha))$, where α is the rotational angle of the shaft. Scroll compression chambers according to this definition are shown in Figure 1. The example shows a 7 cm^3 R744 compressor.

2.4 Inner Geometry

The inner transition between the two regular scroll curves is formed by two tangential arc segments (bi-arc). The radii can be chosen in a specific way to either create perfect-meshing conditions or to open up a gap during the discharge process. Detailed insights into calculating discharge chamber areas are given *e. g.* by Bell (2011) and Blunier *et al.* (2006). These arc segments are also taken into account in the analytical approach by implementing them into the geometric integrals together with the regular scroll curves, if necessary, for certain chambers.

2.5 Exemplary Derivation of Expressions in Closed Form

Deriving closed formulas for geometric features may be tedious at first, but pays off later when numerical approximations are not required. Obvious derivations would include compression chamber areas, including suction and discharge sections, which introduce additional complexity. There also are other results which are required to calculate the force and torque equilibrium conditions of the orbiting scroll properly. One such feature is the compression chamber centroid, which acts as a point of application of the axial gas force. The sum of these forces will create additional over-turning torques, which need to be compensated by the actual required back-pressure. To get finally a closed form equation, multiple derivatives & integrals have to be solved and simplified, for which the Computer-Algebra-Software Mathematica® is used. For example, for the scroll chamber which is bounded only by regular scroll curves **X** and **XN**

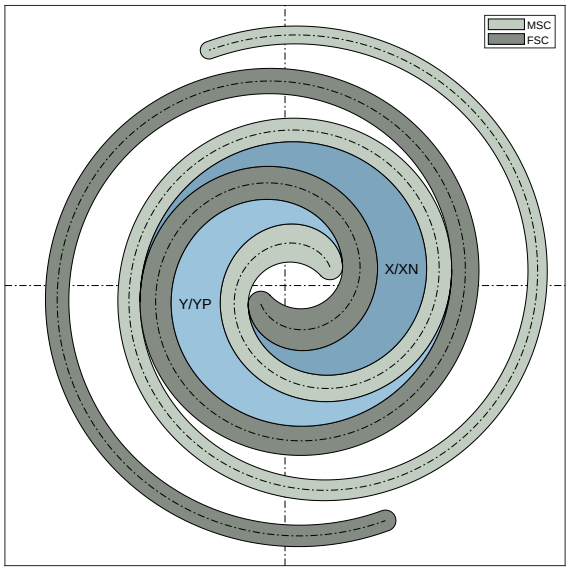

Figure 1: Scroll compressor geometry for R744.

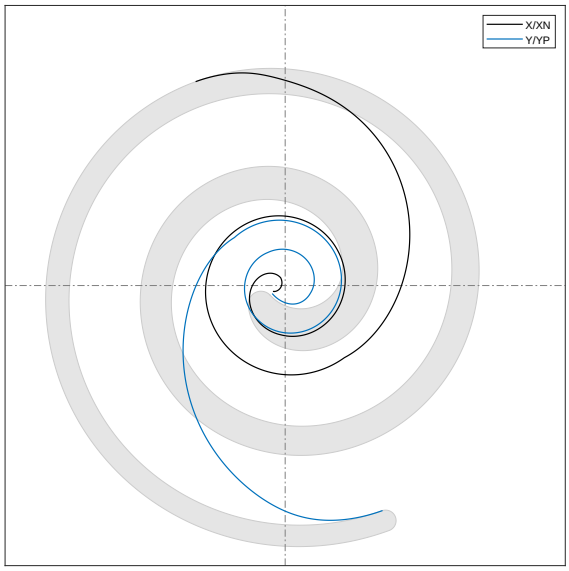

Figure 2: Locus curves of the chamber's center of gravity.

the calculation is done in the following way, applying Green's formalism:

$$A_X(\varphi) = \frac{1}{2}\int_{\varphi}^{\varphi+2\pi} \det\left[\mathbf{X}(u), \mathbf{X}'(u)\right] du \quad = \quad \frac{1}{2}\int_{\varphi}^{\varphi+2\pi} \left(X_x(u)\, X_y'(u) - X_y(u)\, X_x'(u)\right) du \tag{4}$$

where $A_X(\varphi)$ is the area of the polar sector of curve **X** between the tangent angle φ and $\varphi + 2\pi$ of the meshing points. The integral for the corresponding area A_{XN} is calculated in the same way. Furthermore, the sector centroids $\mathbf{X}_C$ and $\mathbf{XN}_C$ of these areas are needed, which *e. g.* is defined for curve **X** as:

$$\mathbf{X}_C(\varphi) = \frac{1}{3\,A_X(\varphi)}\int_{\varphi}^{\varphi+2\pi} \left(\mathbf{X}(u)\, \det\left[\mathbf{X}(u), \mathbf{X}'(u)\right]\right) du \tag{5}$$

The vector to the centroid $\mathbf{C}_{X/XN} = (x_\mathrm{c}, y_\mathrm{c})$ of the chamber area enclosed between curves **X** and **XN** can be obtained by assembling the single results:

$$\mathbf{C}_{X/XN} = \frac{A_X \mathbf{X}_C - A_{XN}\mathbf{XN}_C}{A_X - A_{XN}} \tag{6}$$

As a last step, the explicit equations of the centroid coordinates are derived in Mathematica. The simplified expressions are:

$$x_\mathrm{c} = -\frac{k_1 \cos(\varphi) + k_2 \sin(\varphi)}{k_0} \qquad\qquad y_\mathrm{c} = \frac{k_2 \cos(\varphi) - k_1 \sin(\varphi)}{k_0} \tag{7}$$

with terms

$$\begin{aligned}
k_0 &= 5\left(2a\left(3\varphi^2 + 6\pi\varphi + 4\pi^2 - 6\right) + 6b(\varphi + \pi) + 6c - 3r\right)\\
k_1 &= 30(2a(\varphi + \pi) + b)\left(2a\left(\varphi^2 + 2\pi\varphi + 2\pi^2 - 9\right) + 2b\varphi + 2\pi b + 2c - r\right)\\
k_2 &= a^2\left(15\varphi^4 + 60\pi\varphi^3 + 120\left(\pi^2 - 4\right)\varphi^2 + 120\pi\left(\pi^2 - 8\right)\varphi + 48\pi^4 - 640\pi^2 + 1140\right) + \ldots\\
&\quad 10a\left(3b(\varphi + \pi)\left(\varphi^2 + 2\pi\varphi + 2\pi^2 - 16\right) + c\left(3\varphi^2 + 6\pi\varphi + 4\pi^2 - 18\right) + 6r\right) + \ldots\\
&\quad 5\left(b^2\left(3\varphi^2 + 6\pi\varphi + 4\pi^2 - 15\right) + 6bc(\varphi + \pi) + 3c^2\right)
\end{aligned}$$

The center of gravity of the second chamber $\mathbf{C}_{Y/YP}$ is calculated in the same way. This also represents the general solution for a second-order scroll geometry with variable wall thickness, as indicated above. Similar equations are created for the remaining working chambers, including the suction and discharge areas, which are then implemented together in the software tool using Matlab. To illustrate the result, the path of the entire set of chamber centers of gravity over one revolution is shown in Figure 2.

2.6 Geometric Results

The computation of closed form expressions are carried out for every:

- Chamber areas and area derivatives.
- Area centroids.
- Chamber surfaces (for heat transfer calculations).
- Suction cross sections.
- Resultant gas forces and moments acting on orbiting scroll.

In addition, other closed formulas such as the chamber seal length are used to generate values for the radial and axial clearance of the scroll, which are then used in the 1D simulation model. Despite the aim of calculating as many variables as possible analytically, the discharge cross-sections, for example, can only be determined numerically using Boolean polygon operations. In addition, it is necessary to consider the pressure distribution under the tip faces of the scroll as accurately as possible in order to calculate the required back-pressure. For this purpose, a quadrilateral mesh is automatically created for tip surfaces of the fixed and the orbiting scroll. A corresponding partial differential equation is then solved numerically on the mesh nodes, whereby the pressure boundary conditions of the set of compression chambers are applied to the scroll walls. The PDE utilized for this is the steady-state 2D Laplace equation $\nabla^2\mathbf{u} = 0$, for which the pressures at the tip surfaces are averaged. The numerical solution algorithm uses a finite difference method. Exemplary solutions are shown in Figure 3 & 4. The entire geometric calculation runs on Matlab Parallel Processing Toolbox and takes approximately 0.6 seconds for the selected angular resolution of 0.5°.

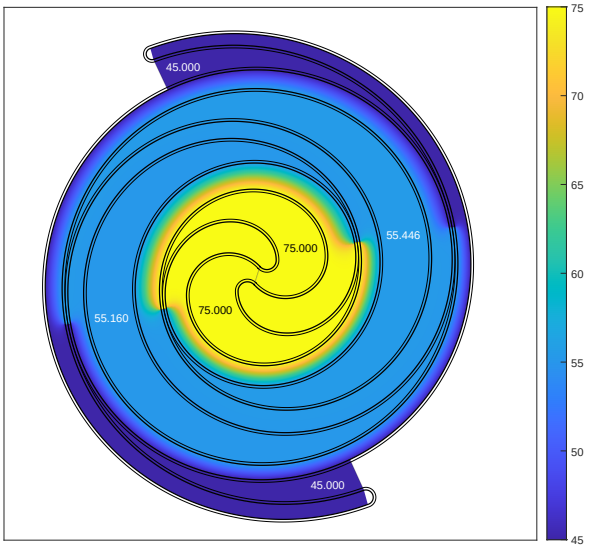

Figure 3: Overall pressure distribution including tip surfaces. Operating point: p_S = 45bar, p_D = 75bar.

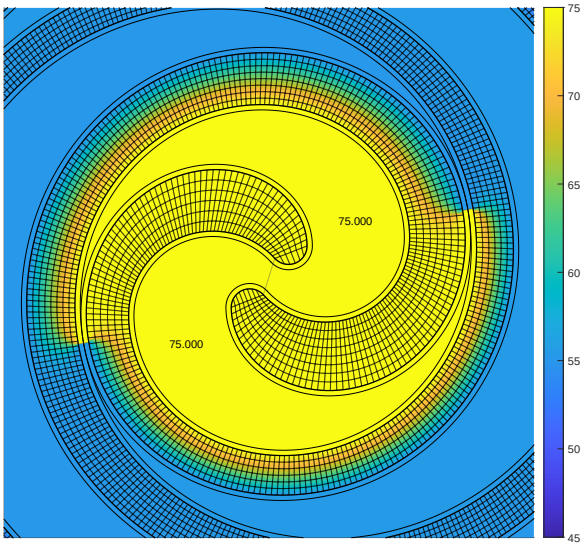

Figure 4: Zoom-in view of Figure 3, showing the quadrilateral mesh of both scrolls.

3. SCROLL COMPRESSOR AXIAL COMPLIANCE

Gas forces during compression are acting to separate orbiting and fixed scroll in axial direction. Without any mechanism to hold them in place, an axial gap between scroll tip surfaces and opposing base-plates would occur ("lift-off"), causing the compression process to either become very inefficient or break down completely. Fixing both scrolls axially at a certain distance is one approach, but it comes with a few drawbacks, *e. g.* tip seals, difficult axial alignment during assembly, and the need for an axial bearing. A more sophisticated way is employing an axial compliance system. Such a system allows small axial movements of the orbiting scroll while loading it with an axial force that constantly pushes it against the fixed scroll, compensating axial tolerances and acting as an axial sealing force. Back-pressure systems are a particular type of axial compliance systems in which the axial force is exerted by a pressurized chamber ("back-pressure chamber") behind the orbiting scroll's base-plate. The pressure in the back-pressure chamber must generally be at a medium level between the low and high pressure of the system. There are several ways in which it can

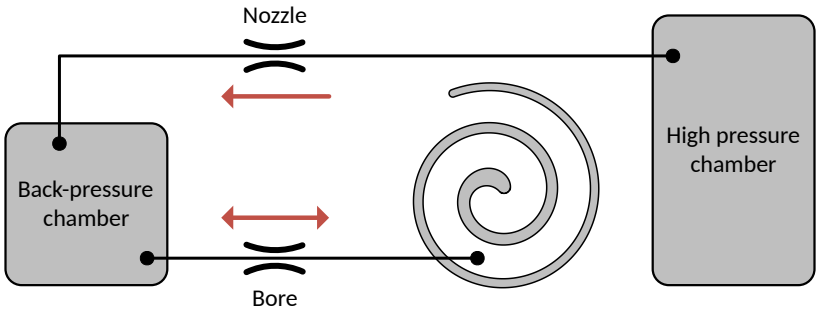

Figure 5: Back-pressure system topology

be regulated using passive or active elements such as nozzles, check-valves or even electrically controlled valves. The simplest variant is to use two individual nozzles that connect back-pressure chamber to low pressure and high pressure chamber. The ratio of the effective diameters of these nozzles determines the level of back-pressure during operation. Two-nozzle systems work well within a narrow range of pressure ratios around the design point. Outside this range, however, the back-pressure becomes either too low (lift-off) or too high (frictional heat, temperature problems, loss of efficiency), making this design unusable in today's automotive scroll compressors with their wide range of pressure ratios (up to 6-7 for R744, up to 15 for typical HC/HFO refrigerants).

3.1 Variable Back-Pressure System for R744 Refrigerant

A way to extend the operating range of the back-pressure system is to replace one nozzle with a bore through the orbiting scroll. This is more complex in terms of simulating and tuning than the previously mentioned two-nozzle system, but direct access to the compression process has significant advantages in system behavior. The focus of this work is on this kind of back-pressure system (see Figure 5). A feed nozzle permanently connects the high-pressure side of the compressor to the back-pressure chamber. Furthermore, a borehole through the MSC connects compression chambers with the back-pressure chamber. This bore can have both a feed or discharge effect, depending on the pressure difference between the chambers at a particular point in time. In contrast to a fixed nozzle, the bore connection is only temporarily open or closed during a section of the compression process as it passes over the wall of the fixed scroll. When designing such a system for a specific scroll contour and refrigerant, an optimum combination of bore position, diameter and fixed nozzle diameter must be found to allow the compressor to operate at any point of its envelope.

4. REQUIRED MINIMUM BACK-PRESSURE

Assuming rigid body mechanics, there are two effects working to separate orbiting from fixed scroll axially. First, the gas pressure inside the scrolls is acting axially on the orbiting scroll, causing a separating force ("axial gas force", see Figure 6a). Second, moments that are acting to tilt the orbiting scroll are supported in a resulting contact point on the fixed scroll. This causes an additional axial force ("axial contact force", see Figure 6b). The force exerted by the back-pressure (see Figure 6c) needs to be at least equal to the sum of axial gas force and axial contact force over an entire 360° period of rotation. The minimum back-pressure level that produces enough axial force to fulfill that condition is called required minimum back-pressure. Since back-pressure is (aside from pulsations of a few kPa) very constant during one revolution, in contrast to the axial forces, excess forces occur which cause unavoidable friction. The amplitude of $F_{\mathrm{BP,req(z)}}$ as shown in Figure 7a should therefore be as low as possible.

4.1 Equilibrium Conditions of Orbiting Scroll

To stabilize the orbiting scroll during one revolution, one has to solve the resultant equilibrium equations to find the required minimum back-pressure force. 3D rigid body equilibrium conditions are used for this purpose, including all gas forces, inertia forces (introduced by D'Alembert's principle) and reaction- as well as gas moments:

$$\sum_{i=1}^{n} \mathbf{F}_i = 0 \qquad \text{and} \qquad \sum_{i=1}^{n} \mathbf{r}_i \times \mathbf{F}_i + \sum_{j=1}^{m} \mathbf{M}_j = 0 \tag{8}$$

The z-coordinate direction is relevant for the back-pressure force. The resulting axial gas force $F_z = F_{z,\mathrm{gas}} + F_{z,\mathrm{tip}}$ consists of two parts, namely the first component $F_{z,\mathrm{gas}}$, which is caused by the respective individual chamber pressures

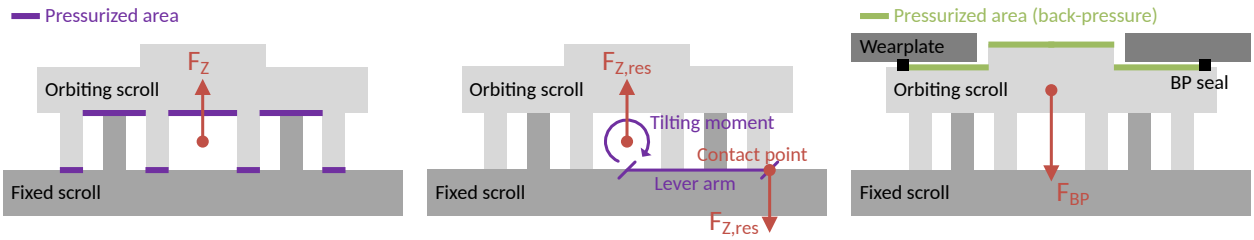

(a) Axial gas force, F_Z **(b)** Axial contact force, $F_{Z,res}$ **(c)** Back-pressure force, F_{BP}

Figure 6: Axial forces acting on orbiting scroll

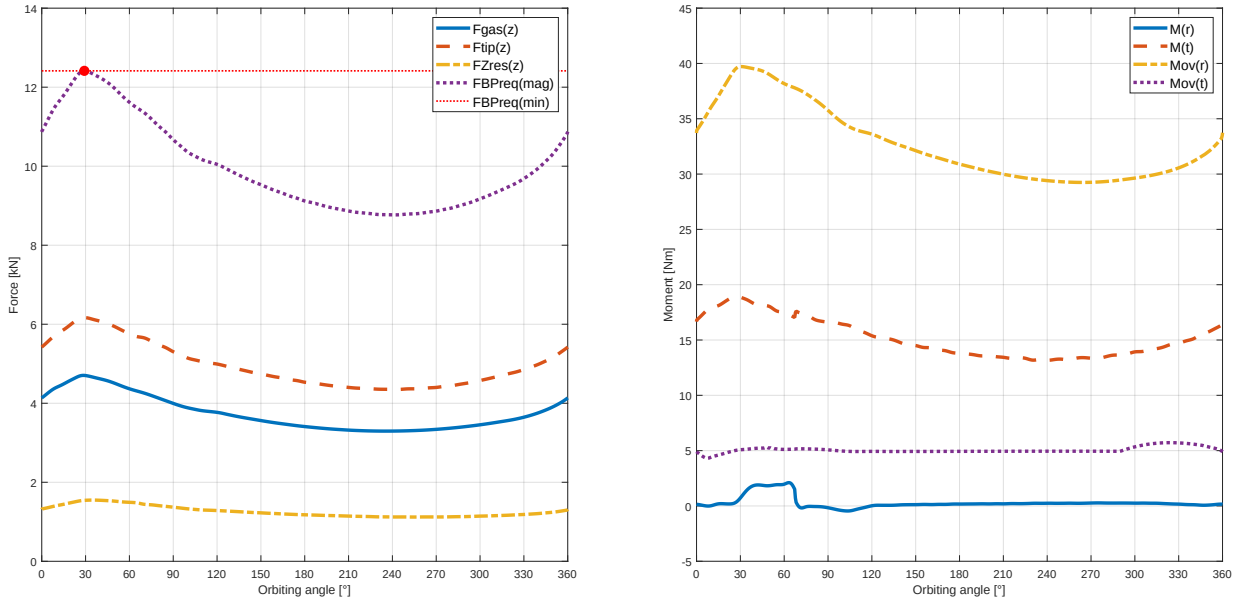

(a) Axial forces **(b)** Gas moment and overturning moment

Figure 7: Orbiting scroll forces & moments acting in a typical R744 operating point (7cm^3 displacement)

acting on their projected surfaces on the orbiting scroll (with the force application point in the chamber's center of gravity), and secondly the component $F_{z,\text{tip}}$, which is caused by the pressure gradient acting under the MSC's tip surface. The axial contact force, $F_{z,\text{res}}$ is affected by radial and tangential gas moments (M_r and M_t) and over-turning moments around the corresponding r and t-axis (M_{or} and M_{ot}). Furthermore, by radial contact force (F_{Rres}), radial anti-rotational force (F_{Rar}) and orbiting scroll centrifugal force (F_{C}) because all of them acting in a plane axially shifted from the origin located at half the scroll's wall height. The contact force is given as:

$$F_{z,\text{res}} = \frac{1}{r_z}\sqrt{(M_r + M_{\text{or}})^2 + (M_t + M_{\text{ot}} - F_{\text{Rres}}\, z_1 + F_{\text{Rar}}\,(z_{\text{ar}} - z_1) + F_{\text{C}}(z_{\text{C}} - z_1))^2} \tag{9}$$

where r_z is the average distance from orbiting scroll center axis (z-axis) to the resulting contact point where moments are supported (see lever-arm in Figure 6b). The axial distance of scroll mid-plane (located at half wall height) to eccentric bearing center is denoted as z_1, the distance to the anti-rotational plane as z_{ar} and to orbiting scroll's center of gravity as z_{C}. Knowing F_z and then $F_{z,\text{res}}$ from equation 9, the required back-pressure force $F_{\text{BP,req}}$ becomes: $F_{\text{BP,req}} = F_z + F_{z,\text{res}}$. Having the MSC's back-pressure seal (see Figure 6c) effective diameter d_{seal}, the required minimum back-pressure – which is defined relative to suction pressure – during one revolution of the compressor is calculated as:

$$\Delta p_{\text{BP,req}} = \max\left(F_{\text{BP,req}}\right)\frac{4}{\pi}\frac{1}{d_{\text{seal}}^2} \tag{10}$$

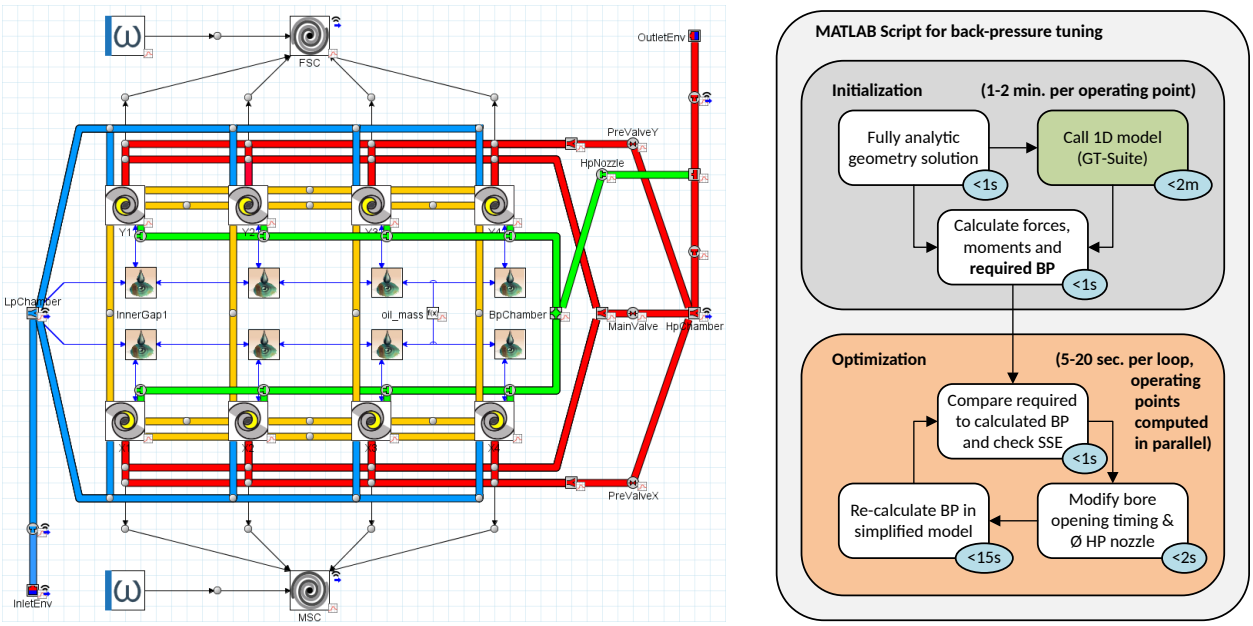

(a) Transient model of compression process in GT-Suite

(b) Toolchain overview

Figure 8: Simulation Environment

5. THERMODYNAMIC MODEL

In order to calculate the forces described in Section 4, the instantaneous pressures in each individual chamber must be known. A 1D thermodynamic model in GT-Suite, a multi-domain simulation platform from Gamma Technologies, was used to calculate them. The proposed analytical geometry approach helps to quickly parameterize the model with all required volume and flow cross-section characteristics.

5.1 GT-Suite® Chamber Model

The top level of the scroll chamber model is shown in Figure 8a. It is a significantly expanded version of the GT-Suite scroll model, which was also shown by Pham, H.-D. *et al.* in 2016 & Harrison *et al.* (2018). The model is called externally from the main program and returns a result file in tabular form. The model is capable of simulating the compression process with relevant physical effects such as internal leakage in radial and axial direction, re-expansion of gas from dead volumes (*e. g.* from discharge bores in the fixed scroll base-plate) as well as discharge reed-valve dynamics. One of the modifications introduces an internal heat exchange model, including electrical and mechanical losses as well as the thermal impact of the refrigerant oil. Including these effects allows for a more accurate prediction of scroll chamber pressure and BP-chamber temperature, which is key to predict the steady-state pressure in the back-pressure chamber with good precision.

In Figure 8a, blue flow paths are linked to suction side, red to discharge side, green to back-pressure chamber and yellow paths represent leakage paths. The eight identical blocks with scroll icons represent individual scroll chambers at different phases of compression. Several of these are needed to model the full scroll compression process with its simultaneously active compression cycles that are phase shifted by 360° intervals.

5.2 Simplified Back-Pressure Model

Re-calculating the back-pressure in each optimization iteration happens in a reduced model that considers just the back-pressure chamber volume with its two flow connections. The simplification consists in assuming that the mass flow rates going in and out of the chamber are small enough to not significantly affect scroll and HP chamber pressure. Therefore, they can be assumed as ideal pressure constraints with pressure data coming from the GT-Suite model. Calculating a new steady-state back-pressure in this model proved to be significantly faster than solving the entire compression process in each loop. Figure 5 is a representation of what this model looks like.

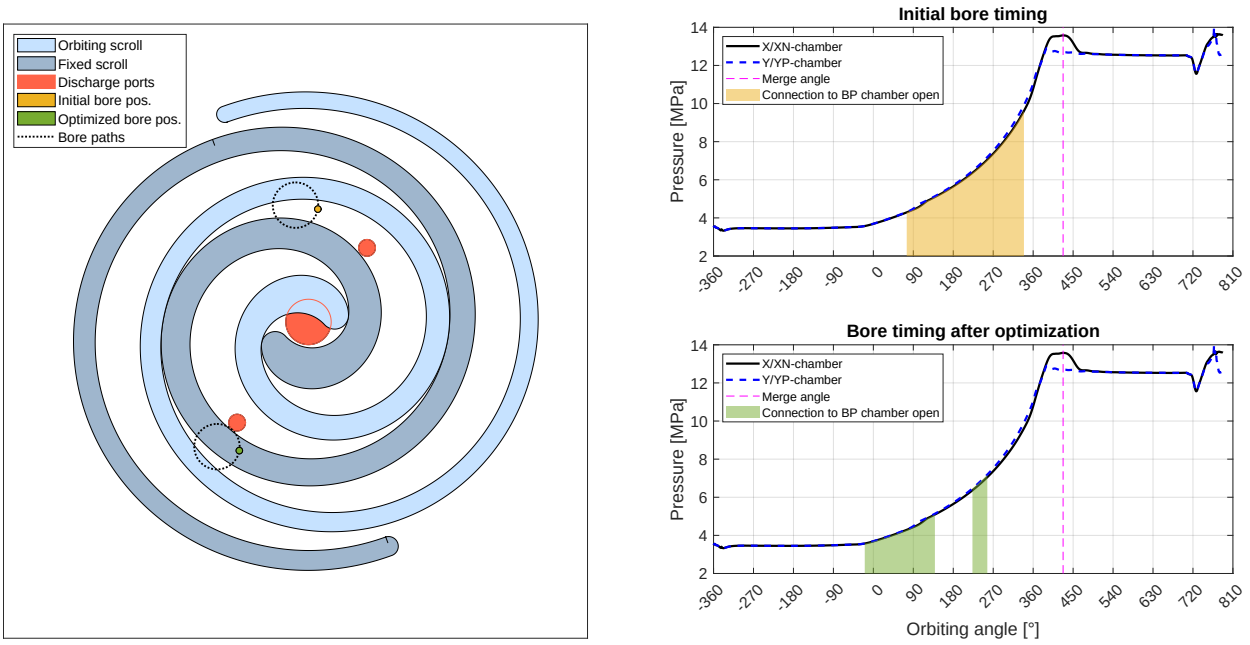

(a) Bore path in 2D space (initial and optimized)

(b) Pressure curves with "bore open" phases

Figure 9: Back-pressure bore position and timing charts

6. OPTIMIZATION

The following section shows how the task of finding a suitable back-pressure configuration is solved. For this purpose, a design layout of the back-pressure system as described in section 3.1 is used as starting point. The optimization problem is finding a suitable position for the bore (two DOFs) and the diameter of the feed nozzle (third DOF), assuming that the diameter of the bore drilled through the orbiting scroll is fixed at 0.3 mm.

6.1 Matlab® Toolchain

The top-level structure of the optimization toolchain is shown in Figure 8b. All subroutines and functions involved are written in Matlab. Two external tools are integrated into the toolchain: NIST REFPROP for the generation of real gas data and GT-Suite for the 1D simulation of the compression process.

Before the optimization can be performed, a required minimum back-pressure for each operating point has to be calculated with the help of the analytic formalism and the GT-Suite model. This step takes around 2 minutes per point. The optimization loop is set up using the minimum search function `fminsearch`. The system's three degrees of freedom serve as tuning variables for the optimizer. In order to limit the bore position to feasible locations, *i. e.* avoiding walls, the analytic approach is used to create a parameter space that lies within the X/XN and Y/YP chamber's border, as seen in Figure 1. In every iteration, a new bore opening function (as seen in Figure 9b) and nozzle diameter are set and serve as input for the reduced back-pressure model (described in Section 5.2). Finally, all selected operating points of the envelope are calculated in a parallel for-loop. Typically, a single iteration of the loop takes between 5 and 20 seconds to complete.

The optimizer's target function is an RMS error residual between the required minimum back-pressure and the actual back-pressure across all operating points. Negative errors, *i. e.* back-pressure is too low, are discarded, since orbiting scroll lift-offs are not acceptable in real operation. Additionally, a final run with the full GT model is performed at the end, in order to update the required minimum back-pressure and verify that the optimization result is still valid.

6.2 Optimization Results

Figure 9a shows both the initial and final location of the orbiting scroll bore in 2D space. Not depicted is the HP nozzle diameter, which the optimizer changed from 0.2 mm to 0.14 mm for the final converged result.

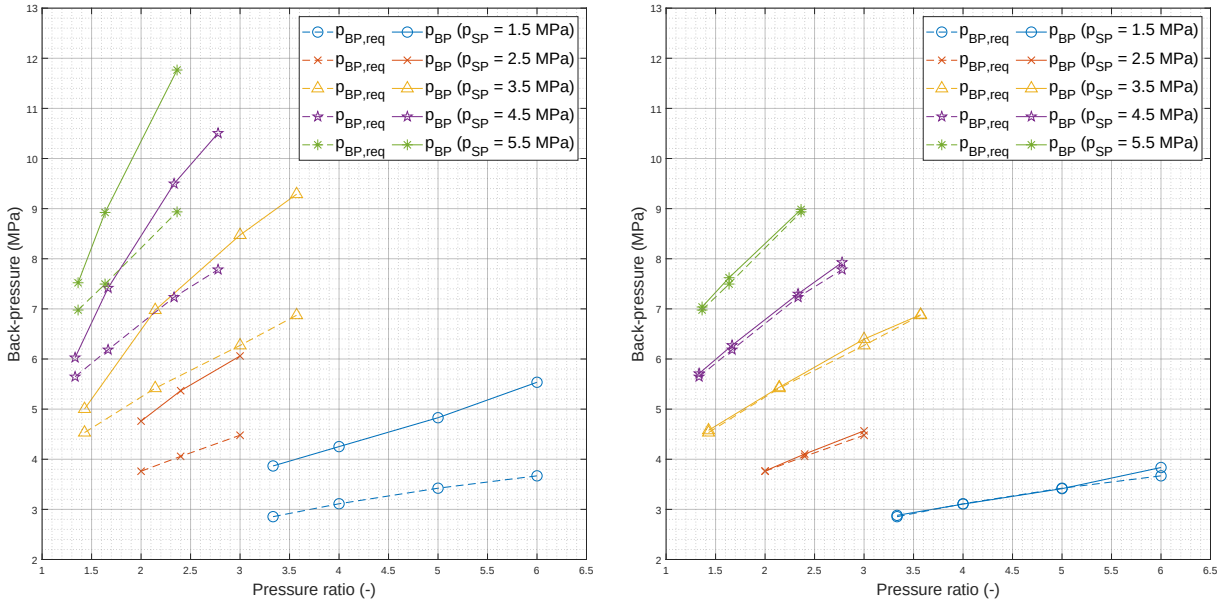

(a) Result with initial (manual) guess

(b) Result after optimization

Figure 10: Optimization results

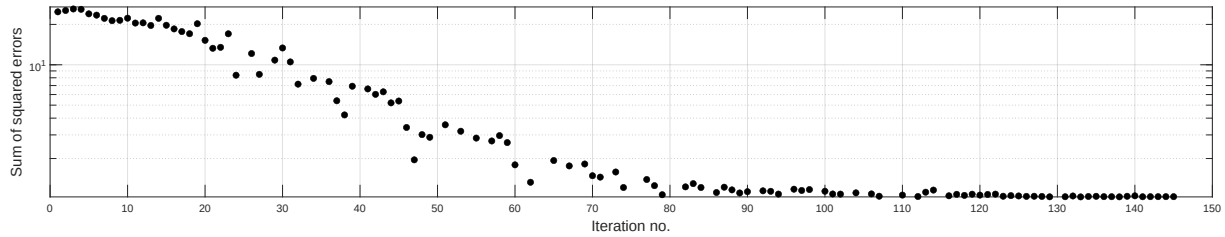

Figure 11: Objective function result (SSE) plotted over iteration count

Figure 10 shows diagrams comparing the required minimum back-pressure and the actual back-pressure within the specified operating envelope. Each color represents a group of points with identical suction pressure. The suction pressure range extends from typical heat pump to battery cooling operation covering evaporation temperatures from -30°C to 20°C. The starting point of the optimization with a manually estimated bore position and nozzle size can be seen in Figure 10a. The actual back-pressures are clearly too high at most operating points. After successful optimization with about 150 iterations, an improved result is reached (see Figure 10b), in which the actual back-pressure lines are very close to the targeted ones. The optimized bore position and nozzle diameter result in calculated deviations within 0.1 MPa, which is the necessary target region to be achieved for an R744 scroll compressor and a good starting point for testing on real hardware. The chart in Figure 11 shows the objective function's values of each iteration of `fminsearch` until converging to its final value. The entire calculation took around 45 minutes to complete on an Intel Core i9 13900K CPU.

7. CONCLUSIONS

This work presents a toolchain to create, simulate and automatically fine-tune variable back-pressure systems for scroll compressors. An analytical mathematical approach enables the full description of a scroll contour geometry by explicit formulas, which then provide geometric input data for a 1D thermodynamic model that simulates the compression process.

The result of this 1D model, *i. e.* the instantaneous chamber pressure of each individual chamber, is then used in analytical formulas for the chamber area and center of gravity to obtain the resulting gas forces and gas moments. These

are subsequently used to calculate a required minimum back-pressure level for each operating point, which serves as a reference for tuning the back-pressure system. The back-pressure is tuned using a minimum search function in Matlab. It optimizes the position of a bore in the orbiting scroll and the diameter of a feeding nozzle. The analytical geometry description in conjunction with a reduced back-pressure chamber model helps to keep the overall calculation time at a minimum and ultimately achieve deviations of less than 0.1 MPa from the optimum target.

With an accurate, calibrated thermodynamic model, the back-pressure behavior of the machine can be predicted well enough for it to function stably at the vast majority of operating points. This greatly reduces the time spend on fine-tuning the feeding nozzle size on real hardware. It also reduces the risk of having to resort to costly and time-consuming hardware changes, such as repositioning the bore on an orbiting scroll during prototype validation.

NOMENCLATURE

F	force	(N)
M	torque	(Nm)
p	pressure	(MPa, absolute)

Subscript

MSC	moving (orbiting) scroll
FSC	fixed scroll
HP	high pressure (discharge)
SP	suction pressure
BP	back-pressure
RMS	root mean square
ar	anti-rotation
C	centrifugal
res	resultant (sum of all chambers)
req	required
r	in radial direction
t	in tangential direction
z	in axial direction

REFERENCES

Bell, I. (2011). *Theoretical and experimental analysis of liquid flooded compression in scroll compressors* (PHD Thesis). Ray W. Herrick Laboratories, Purdue University.

Bell, I., Groll, E., Braun, J., & King, G. (2010). Update on scroll compressor chamber geometry. *20th International Compressor Engineering Conference (No. 1489), Purdue University*.

Blunier, B., Cirrincione, G., & Miraoui, A. (2006). Novel geometrical model of scroll compressors for the analytical description of the chamber volumes. *18th International Compressor Engineering Conference (No. C074), Purdue University*.

Creux, L. (1905). *Rotary engine.* (U.S. Patent No. 801182)

Gravesen, J., & Henriksen, C. (2001). The geometry of the scroll compressor. *SIAM Review*, *43*(1), 113–126.

Harrison, J., Koester, S., Aihara, R., & Ratner, D. (2018). From CAD to 1D: A direct approach to modeling scroll compressors with multi-physics simulation. *24th International Compressor Engineering Conference (No. 1190), Purdue University*.

Nieter, J., Marchese, A., & DeBlois, R. (1992). Dynamic axial compliance to reduce friction between scroll elements. *Proceedings of the 1992 International Compressor Engineering Conference at Purdue*, 1107–1116.

Ooi, K., & Han, W. (1996). Optimizing the back pressure port of a scroll compressor. *1996 International Compressor Engineering Conference. Paper 1164*.

Pham, H.-D., & Lehocky, M. (2016). Modeling of scroll compressor using GT-Suite. *2016 GT User Conference*.

Shaffer, B., & Groll, E. (2012). Parametric representation of scroll geometry with variable wall thickness. *21st International Compressor Engineering Conference (No. 1268), Purdue University*.

Tojo, K., Ikegawa, M., Maeda, N., Machida, S., & Shilbayashi, M. (1986). Computer modeling of scroll compressor with self adjusting back-pressure mechanism. *Proceedings of the 1986 International Compressor Engineering Conference at Purdue*, 872–886.